

Effect of Solid Particle Density on Hydraulic Performance of a Prototype Sewage Pump

Xiao-Jun Yang¹, Yu-Liang Zhang², Zhen-Gen Ying³, Yan-Juan Zhao⁴

^{1,2,3}College of Mechanical Engineering, Quzhou University, Quzhou 324000, China

⁴College of Information Engineering, Quzhou College of Technology, Quzhou 324000, China

Abstract— A frozen rotor method based on a mixture multiphase flow model, an RNG $k-\epsilon$ dual-equation turbulence model, and a SIMPLE algorithm is used to perform a numerical simulation of steady flow in a sewage pump that transports solid and liquid phase flows. The method is also utilized to analyze the effect of solid-phase particle density on the hydraulic performance of the sewage pump and predict the wear degree of the overflow components. Results of the study indicate that with the increasing density of solid particles, the head curve of the pump initially decreased and then increased, that is, the head curve had the minimum value. Additionally, the efficiency curve of the pump increased, decreased, and then increased again, indicating an insignificant overall change. Meanwhile, the pump shaft power showed a monotonic upward trend. When the solid-phase density is less than, equal to, and greater than the liquid-phase density, solid-phase concentration on the blade pressure surface shows a distribution law more than, equal to, and less than 10%, respectively. With the increase in density of the delivered solid particles, solid-phase concentration on the blade pressure surface shows a decreasing trend.

Keywords— sewage pump, particle density, frozen rotor method, numerical calculation.

I. INTRODUCTION

Sewage pumps consist of both solid- and liquid-phase flow pumps and are key equipment for urban channel cleanout. Many scholars at home and abroad have carried out in-depth and meticulous research on sewage pumps and have achieved productive results. Engin et al considered a centrifugal pump with a semi-closed impeller as the object of study to compare the performance of the pump in delivering water, sand, and other media with different hardness. They likewise provided a conclusion regarding the relationship between particle size and pump performance. The deviation between predicted and measured values of the solid- and liquid-phase head of delivery was $-20\sim+15\%$ [1]. Gandhi et al. carried out an experimental study on the performance of a centrifugal pump with a closed impeller in delivering water, mortar, and a solid-liquid mixture of zinc tailings. When the solid concentration was smaller than 20%, the relationship between the pump head and the flow could be confirmed through the relational expression of the water's working conditions. When the solid concentration was higher than 20%, the effect of solid particles on the pump performance should be considered [2]. Yuan et al. carried out a numerical simulation of solid-liquid two-phase turbulence inside a non-overloaded mud pump [3]. Findings suggested that backflow occurred in the inlet and velocity slip between two phases, and turbulent kinetic energy and dissipation rates reached their peaks at the junction of the pressure surface and the suction surface. Li et al. conducted an experimental study on the effect of solid particle properties, including concentration and particle size, on the external characteristics of centrifugal pumps [4]. Under the working condition of small flow, efficiency value increased slightly, the stable working area decreased, and the optimal efficiency point moved to the small flow direction. Zhang et al. performed a numerical research on solid-liquid two-phase flow field in a low specific speed centrifugal pump by means of numerical calculation [5]. The obvious jet flow-wake structure occurred near a volute tongue, and it was more obvious with the increase of volume fraction. Zhang et al. made a numerical simulation of the start-up characteristics of a high specific speed centrifugal pump for solid-liquid two-phase flow by means of a dynamic grid [6]. Harry et al. carried out an experimental study on a centrifugal pump blade made of high chromium white iron and aluminum alloy through a Coriolis experiment [7] to obtain different wear modes on the centrifugal pump blade as it delivers mud. Veselin et al. put forward a new wear prediction method based on a fast experiment and mathematical analysis [8] to substitute a costly and time-consuming traditional slurry pump wear test with weak applicability. The error between the predicted results and the experimental results was less than 3%. Pagalthivarthi et al. studied the effects of operational parameters, pump flow and velocity, particle diameter, different geometries, curve of tongue, and width of volute on erosion wear on particles through a numerical calculation [9]. Dong et al. conducted a study and found that particle size and shape, liquid velocity, and other flow parameters had a great impact on erosion pit on the surface of wet parts, and that the degree of distortion and maximum stress of the pit increased with the increase of particle size [10]. Li et al. revealed the impact of internal flow characteristics on the wear characteristics of solid-liquid two-phase centrifugal pump [11].

Therefore, studying the internal flow of the pump to provide a theoretical basis for realizing a high-performing and stable-operating pump design is needed. The present study aims to conduct a numerical simulation and analysis on solid-liquid two-phase flow pump to analyze the impact of the density of solid-phase particles on sewage pump performance, including the hydraulic performance of sewage pump and wear degree of wet parts.

II. PUMP MODEL AND CALCULATION METHOD

2.1 Pump model and computational grid

The pump model used for the computation was a medium specific speed centrifugal pump, with a specific speed of $n_s=129.3$. Its basic performance parameters were as follows: flow rate $Q=50\text{m}^3/\text{h}$, head $H=20.54\text{m}$, velocity $n=2900\text{r}/\text{min}$, shaft power $P_a=3.54\text{kW}$, efficiency $\eta=79.5\%$ and net positive suction head $NPSH_C=2.59\text{m}$. The main dimensions of the pump were as follows: inlet diameter $D_j=76\text{mm}$, hub diameter $d_h=0\text{mm}$, impeller outlet diameter $D_2=137\text{mm}$, impeller outlet width $b_2=14\text{mm}$, blade outlet angle $\beta_2=30^\circ$, blade number $Z=6$, blade wrap angle $=104.5^\circ$, volute base circle diameter $D_3=145\text{mm}$, and volute inlet width $b_3=30\text{mm}$.

2.2 Computational grid

The commercial software UG was used to create a 3D model of the internal computing area. The appropriate extension of the straight-tube suction chamber was made to eliminate the influence of the given inlet speed. An appropriate extension of the pump outlet was also carried out to better calculate convergence. As shown in Fig.1, the commercial grid partitioning software GAMBIT2.3.16 was used to create a grid division of the computational domain. Tetrahedral meshes were adopted in the impeller rotation region and volute static region, with mesh numbers 435,530 and 597,127 respectively. Hexahedral meshes were used in the suction chamber and outlet extension, with mesh numbers of 152,827 and 54,944 respectively. The total mesh number of the overall computational domain was 1,240,428. This number was not enough to simulate the micro flow in the boundary layer of simulation but was sufficient for the macro flow and macro characteristic capturing in the pump. Mesh quality checking revealed that the equiangular slope and equidimensional slope of the mesh were not more than 0.83. Mesh quality was good at around 30 near wall Y+.

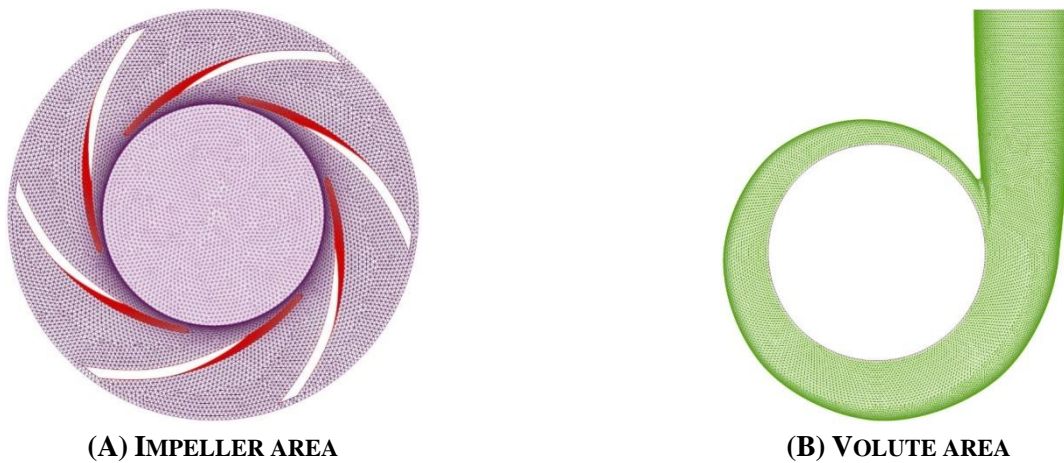


FIG.1 COMPUTATIONAL MESH

2.3 Governing equations

The 3D unsteady turbulent flow of incompressible fluid in a centrifugal pump can be described by Reynolds-averaged equations.

$$\left\{ \begin{array}{l} \frac{\partial \bar{u}_i}{\partial x_i} = 0 \\ \rho \frac{\partial \bar{u}_i}{\partial t} + \rho \bar{u}_j \frac{\partial \bar{u}_i}{\partial x_j} = \rho F_i - \frac{\partial \bar{p}}{\partial x_i} + \mu \frac{\partial^2 \bar{u}_i}{\partial x_j \partial x_j} - \rho \frac{\partial}{\partial x_j} \left(\overline{u_i u_j} \right) \end{array} \right. \quad (1)$$

Where ρ refers to fluid density, and $-\rho \overline{u_i u_j}$ refers to mean Reynolds stress.

Unsteady turbulent flow calculation used in the present study used the RNG $k-\varepsilon$ two-equation model to close the mean Reynolds stress. RNG $k-\varepsilon$ turbulent model, which considers the rotation and swirling flow in the mean flow, can better process the flow with high strain rate and great streamline curvature.

2.4 Multiphase flow model

This study aims to make a 3D turbulent flow calculation of incompressible viscous fluid by using the commercial code FLUENT software based on a finite volume method. The multiphase flow model in numerical computation used the algebraic slip mixture model [12] based on Euler's method to complete the calculation of solid-liquid two-phase flow. In the calculation, the particles were treated as quasi fluid.

2.5 Solution settings

The dynamic and static coupling between rotor and stator in numerical calculation was achieved by means of the frozen rotor method. Velocity inlet and free output were respectively used as the boundary conditions of the inlet and outlet. No-slip boundary condition was applied on all solid walls considering viscosity, and standard wall function was used in near-wall low Reynolds number region to deal with the problem from the high Reynolds number turbulence model. The coupling between velocity and pressure was calculated by using SIMPLE algorithm. First-order upwind scheme was used for the spatial discretization of the convection term. The central difference scheme with two-order accuracy was used for the spatial discretization of diffusion terms. The linear standard format was used for spatial discretization of the source terms considering that solid particles were uniform spherical particles with unchanged physical properties. The convergence criterion of each control equation was 0.0001.

2.6 Computational scheme

To explore the effect of solid-phase properties on hydraulic transport performance as the sewage pump delivers solid-liquid two-phase flow, the following computational scheme was formulated:

Under a designed flow rate ($Q=50\text{m}^3/\text{h}$) with 10% solid-phase concentration and 0.10mm particle diameter, numerical calculation was conducted for a solid-liquid two-phase flow field under five conditions when the particle densities were 500, 1000, 1500, 2000, and 2500 kg/m^3 .

III. ANALYSIS OF RESULTS

3.1 External characteristics

Pump inlet and outlet pressures and the external characteristics under five particle densities obtained from the numerical calculation are shown in Figs.2 and 3. In Fig. 2, the densities of solid particles in delivering solid-liquid two-phase flow were 500, 1000, 1500, 2000, and 2500 kg/m^3 . The values of total pressure at pump inlet were -0.259, -0.281, -0.302, -0.323, and -0.358 kPa, respectively, and the values of total pressure at pump outlet were 128.582, 133.377, 138.662, 146.071, and 153.524, respectively. With the increase of the density of solid particles, the total pressures of the pump inlet and of the pump outlet showed a trend of monotonic decline and rising. The calculation result of external characteristics in Fig.3 shows that when the densities of solid particles in solid-liquid two-phase flow were 500, 1000, 1500, 2000, and 2500 kg/m^3 , the calculated heads were 14.00, 13.80, 13.66, 13.74, and 13.81, respectively, and the calculated efficiencies were 47.02%, 47.17%, 47.097%, 47.36%, and 47.49%, respectively. The calculated shaft powers were 3.850, 3.982, 4.145, 4.344, and 4.551 kW, respectively. With the increase of the density of solid particles, the pump head curve showed an initially decreasing then increasing trend and reached the minimum value of 13.66m when the density of solid particles was 1500 kg/m^3 . The pump efficiency curve showed an initially increasing then decreasing trend. Nevertheless, the absolute value of the overall change was not significant. At the same time, pump shaft power showed a monotonic upward trend.

Previous research has shown that under the assumption of non-viscous and non-granular force, the equation met by solid-liquid two-phase flow in the impeller is deduced theoretically. Based on the conclusion, the pump head delivering two-phase flow was lower than the head delivering liquid-phase flow when the particle density was more than the liquid-phase density. On the contrary, the pump head increased. The calculation results in this study proved that the conclusion is completely correct.

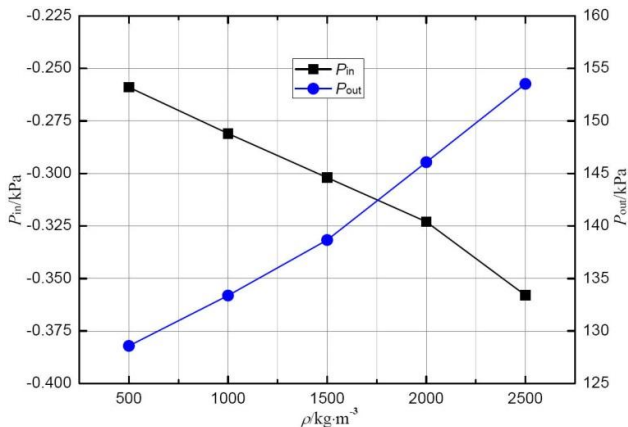


FIG.2 EFFECTS OF PARTICLE DENSITY ON PUMP INLET AND OUTLET PRESSURES

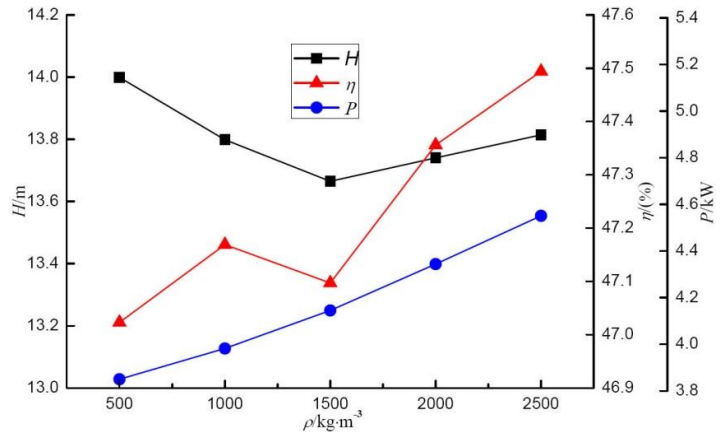


FIG.3 EFFECTS OF PARTICLE DENSITY ON THE EXTERNAL CHARACTERISTICS OF THE PUMP

3.2 Pressure surface characteristics

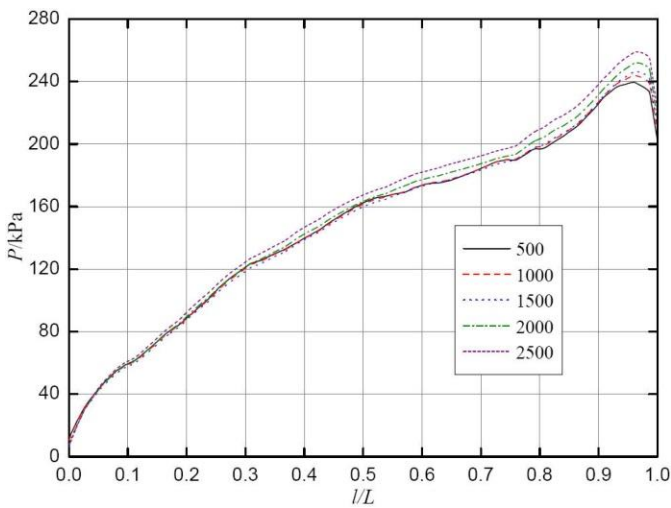
The effects of the density of solid particles obtained from the numerical calculation on the performance parameters of blade pressure surface are shown in Fig.4. Fig. 4(a) shows the influence of total pressure distribution along the blade. The total pressure on the blade pressure surface increased with the increase of the semi diameter. Findings also showed that the second half of the blade pressure surface was the main point of the increase in pressure. Meanwhile, with the increase of the density of solid particles, total pressure on the blade pressure surface showed a gradual increasing trend. The corresponding densities of solid particles were 500, 1000, 1500³, 2000, and 2500kg/m³. In the front of the blade pressure surface, the total pressures were 11.488, 10.490, 7.918, 6.820, and 6.419kPa, respectively. When the relative length of the middle of blade was 0.5, total pressures were 162.641, 161.726, 160.032, 163.475, and 167.60kPa. In the tailing of the blade pressure surface, total pressures were 202.057, 207.212, 209.95, 215.042, and 221.334kPa. In the tailing of the blade pressure surface, total pressure drop occurred due to the influence of jet-wake flow.

Fig. 4(b) shows the obtained distribution of solid-phase concentration on the blade pressure surface. Under different densities of delivering particles, the solid-phase concentration on the blade pressure surface showed a completely opposite distribution status. In the case of particle density (500 kg/m³), the density of solid-phase concentration was smaller than the density of delivering medium water (1000kg/m³). The solid-phase concentration on the blade pressure surface was more than 10% because when particle density is lighter than water, particles suspend in the water medium. Under centrifugal force and blade force, solid particles suspended in the water medium gather on the blade pressure surface, causing solid-phase concentration to significantly increase from the front edge of the blade. Findings indicated that, in this case, the blade pressure surface bore more severe dynamic attacks and wears. However, in consideration of the small density of solid particles, wear degree will be further studied. In the front edge, middle, and tailing of the blade pressure surface, instantaneous solid concentrations were 10.382%, 16.544%, and 12.257%, respectively. When the delivered solid-phase density was 1000kg/m³, solid-phase density was completely equal to water density, and solid phase was equal to water medium. These factors were completely mixed together and suspended. Therefore, the calculation result showed that the solid-phase density on the overall blade pressure surface is always about 10%, which is equal to the calculated solid-phase density of the incoming flow. Findings revealed that the wear on the blade pressure surface was completely similar. In three cases, the densities of solid particles were 1500, 2000, and 2500kg/m³. Starting from the front edge of the blade pressure surface, the concentration of solid-phase particles gradually decreased and dynamically stabilized. Solid-phase concentration was smaller than 10%, which indicated that, in these three cases, the wear on the blade pressure surface was not severe. Large densities of particles also entailed large inertial force of particles. Although particle concentration was not high, a greater degree of wear still occurred. This finding needs further confirmation. In the three cases presented, the instantaneous solid-phase concentrations in the front edge of the blade pressure surface were 9.878%, 10.048%, and 10.187%, respectively. In the middle of the blade pressure surface, instantaneous solid-phase concentrations were 6.15%, 4.48%, and 3.343%, respectively. In the tailing of the blade pressure surface, instantaneous solid-phase concentrations were 8.275%, 7.536%, and 6.908%, respectively. With the increase in density of delivering solid particles, solid-phase concentrations on the blade pressure surface showed a gradual declining trend. This finding indicated that the degree of wear increasingly lessened, which was mainly related to the inertial

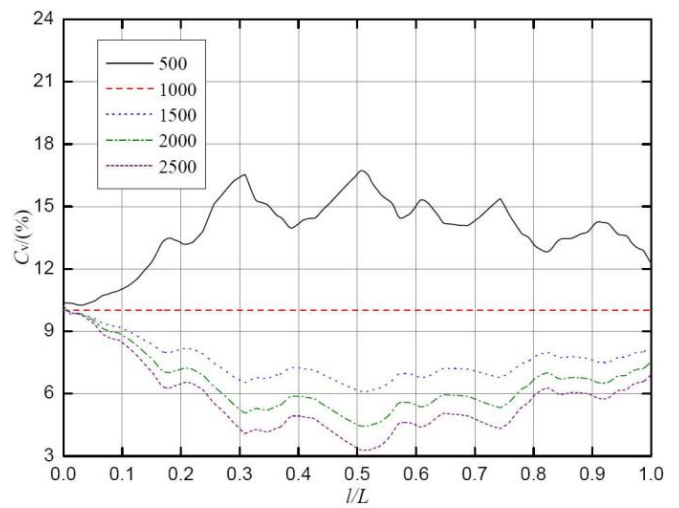
force of solid particles. If the inertial force was greater, the ability of particles to escape from the restraint of the blade pressure surface would be stronger; otherwise, it would be weaker.

In terms of vorticity [Fig.4(c)], the densities of solid particles in five cases were 500, 1000, 1500, 2000, and 2500 kg/m³, respectively. At position 0.2, which was relatively long from the front edge of the blade pressure surface, the obtained vorticity values were 4723.99, 5467.7, 5922.38, 6000.75, and 6016.79 s⁻¹; at position 0.5, the obtained vorticity values were 4998.75, 6544.94, 7552.63, 7804.41, and 7883.16 s⁻¹, respectively; and at position 0.8, the obtained vorticity values were 8780.93, 9692.48, 10462.4, 10838.3, and 10958 s⁻¹, respectively. With the increase in density of delivering particles, the vorticity value on the blade pressure surface showed an increasing trend.

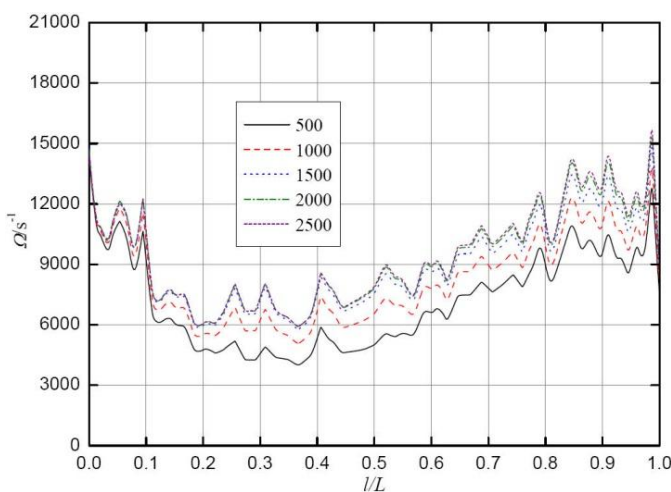
For turbulent kinetic energy [Fig.4 (d)], turbulent dissipation rate [Fig.4(e)], and turbulence intensity [Fig.4(f)], the changing characteristics were generally consistent. In five cases, the densities of delivering solid particles were 500, 1000, 1500, 2000, and 2500 kg/m³, respectively. At position 0.5, which was relatively long from the front edge of the blade pressure surface, turbulent kinetic energies were 4.36109, 3.18985, 2.20454, 1.66049, and 1.28034 m²·s⁻², respectively; turbulent dissipation rates were 22872.9, 14340.3, 8247.05, 5389.18, and 3650.25 m²·s⁻³, respectively; and turbulence intensities were 1.636%, 1.395%, 1.164%, 1.015%, and 0.897%. With the increase in density of delivering solid particles, the turbulence effect on blade pressure surface decreased gradually, and flow was more stable. However, in terms of any kind of delivery concentration, turbulent kinetic energy, turbulent dissipation rate, and turbulence intensity, the minimum value from the front edge gradually decreased and then increased.



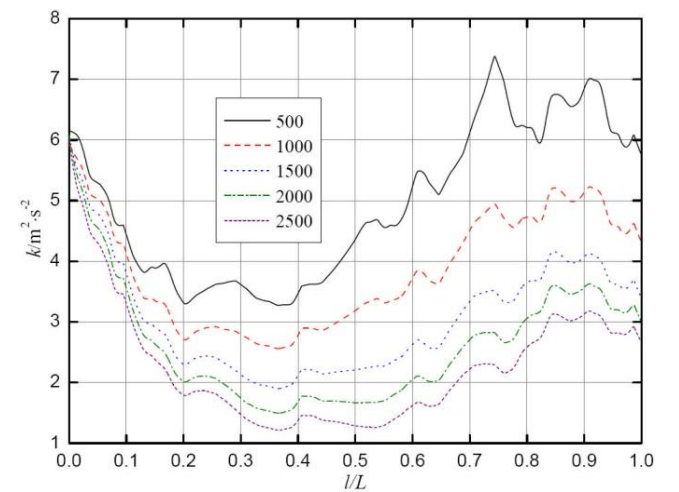
(A) TOTAL PRESSURE



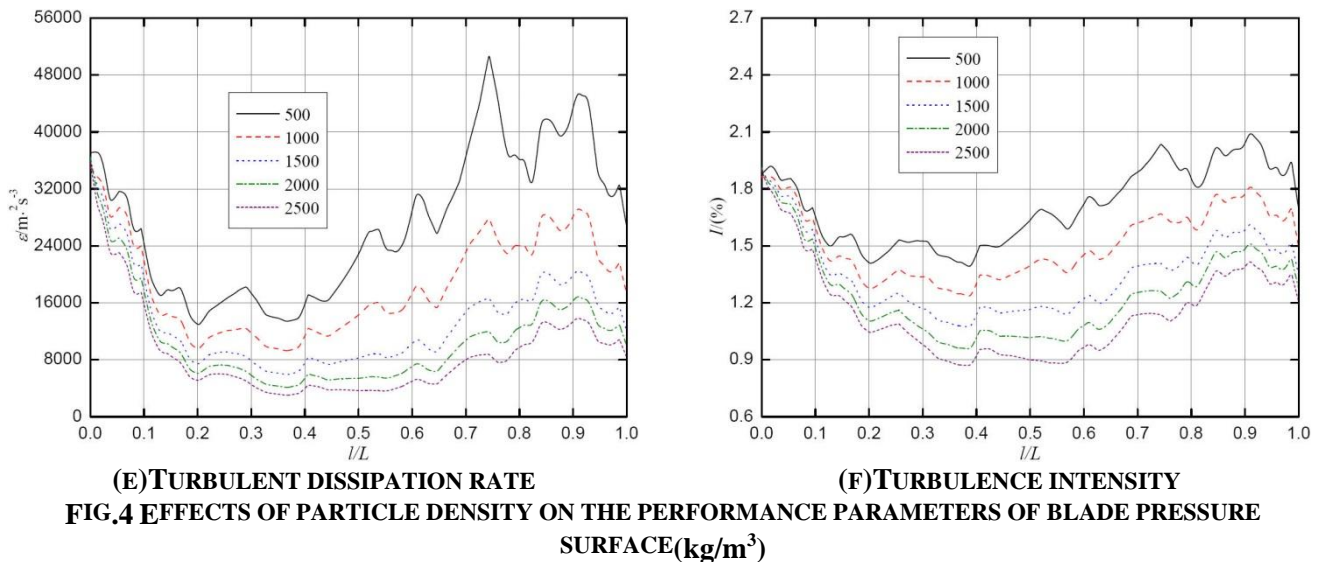
(B) SOLID-PHASE CONCENTRATION



(C) VORTICITY



(D) TURBULENT KINETIC ENERGY



3.3 Suction surface characteristics

The effect of the density of solid particles obtained from the numerical calculation on the performance parameters of the blade suction surface is shown in Fig.5. Fig.5 (a) shows the influence of total pressure on the distribution along the blade. For any density of delivered solid particles, total pressure increased from the front edge of the suction surface with the constant increase of the blade's semi-diameter. At the place near the outlet of the suction surface, a sudden drop phenomenon occurred similar to the previous occurrence. In five cases, the densities of delivering solid particles were 500, 1000, 1500, 2000, and 2500 kg/m^3 , respectively. At position 0.10, which was relatively long from the front edge of the blade suction surface, the obtained total pressures were -5.459, -6.553, -7.449, -8.192, and -9.021 kPa, respectively. At position 0.40, the obtained total pressures were 35.215, 35.728, 35.469, 35.593, and 35.880 kPa, respectively. In the scope of 0.4, which was in the first half of the blade suction surface, the effect of the variation in the solid particle densities on the rise of total pressure was not significant. In the scope apart from this site, the total pressure on the blade suction surface showed an increasing trend with the increase in the density of delivering solid particles, in which the density of solid particles mainly affected the second half of the blade suction surface. At position 0.70, the obtained total pressures were 125.945, 142.46, 160.267, 176.806, and 190.735 kPa, respectively. At position 0.90, the obtained total pressures were up to 208.003, 235.989, 269.077, 306.533, and 339.416 kPa, respectively.

The effect of the density of delivering solid particles obtained from the numerical calculation on the distribution of solid-phase concentrations on the blade suction surface are shown in Fig. 5(b). In terms of the medium with the 1000 kg/m^3 density of delivering particles, the solid-phase concentration on the blade suction surface obtained from the calculation was 10%. Apparently, the reason for this finding was that the solid-phase density was the same as the liquid-phase density. When both of these factors had the same density, the solid phase was equal to the liquid phase, free and uniformly distributed. However, in the following four cases, the densities of solid particles were 500, 1500, 2000, and 2500 kg/m^3 before and after the position that was relatively 0.25 long from the front edge of the blade suction surface; the distribution laws of solid-phase concentration were completely opposite. Before position 0.25, the solid-phase concentrations on the blade suction surface showed a declining trend with the increase of the density of solid particles, and after position 0.25, solid-phase concentrations on the blade suction surface showed an increasing trend with the increase of the density of solid particles. For example, at position 0.10, the solid-phase concentrations on the blade suction surface in the above four cases were 11.229%, 8.724%, 7.963%, and 7.338%, respectively; and at position 0.80, the solid-phase concentrations on the blade suction surface in the above four cases were 5.868%, 19.458%, 28.393%, and 32.351%, respectively. In the middle and late parts on the blade suction surface, solid-phase concentrations on the blade suction surface gradually reduced when the density of solid particles was smaller than that of water. This finding indicated that the degree of wear also constantly decreases. Under the condition that the density of solid particles was greater than water density, solid-phase concentrations on the blade suction surface gradually increased. This result indicated that the degree of wear constantly increases. However, in the small part from the front edge of the blade suction surface, the changing trends of both these factors were opposite, revealing that the degrees of wear were also opposite.

Fig.5(c) shows the vorticity distribution on the blade suction surface in cases of different densities of delivering solid particles. Vorticity distribution characteristics in five kinds of delivering density were basically the same, showing a gradually declining trend from the front edge of the blade suction surface. Furthermore, the effect of different densities on vorticity values was not significant. Figs.5(d), 5(e), and 5(f) show the respective distributions of turbulent kinetic energy, turbulent dissipation rate, and turbulence intensity along the blade suction surface under different densities of delivering solid particles. Generally, these factors had similar changing characteristics, namely, increasing with the increase of the densities of delivering solid particles. Three parties reflected time-averaged characteristics of turbulence.

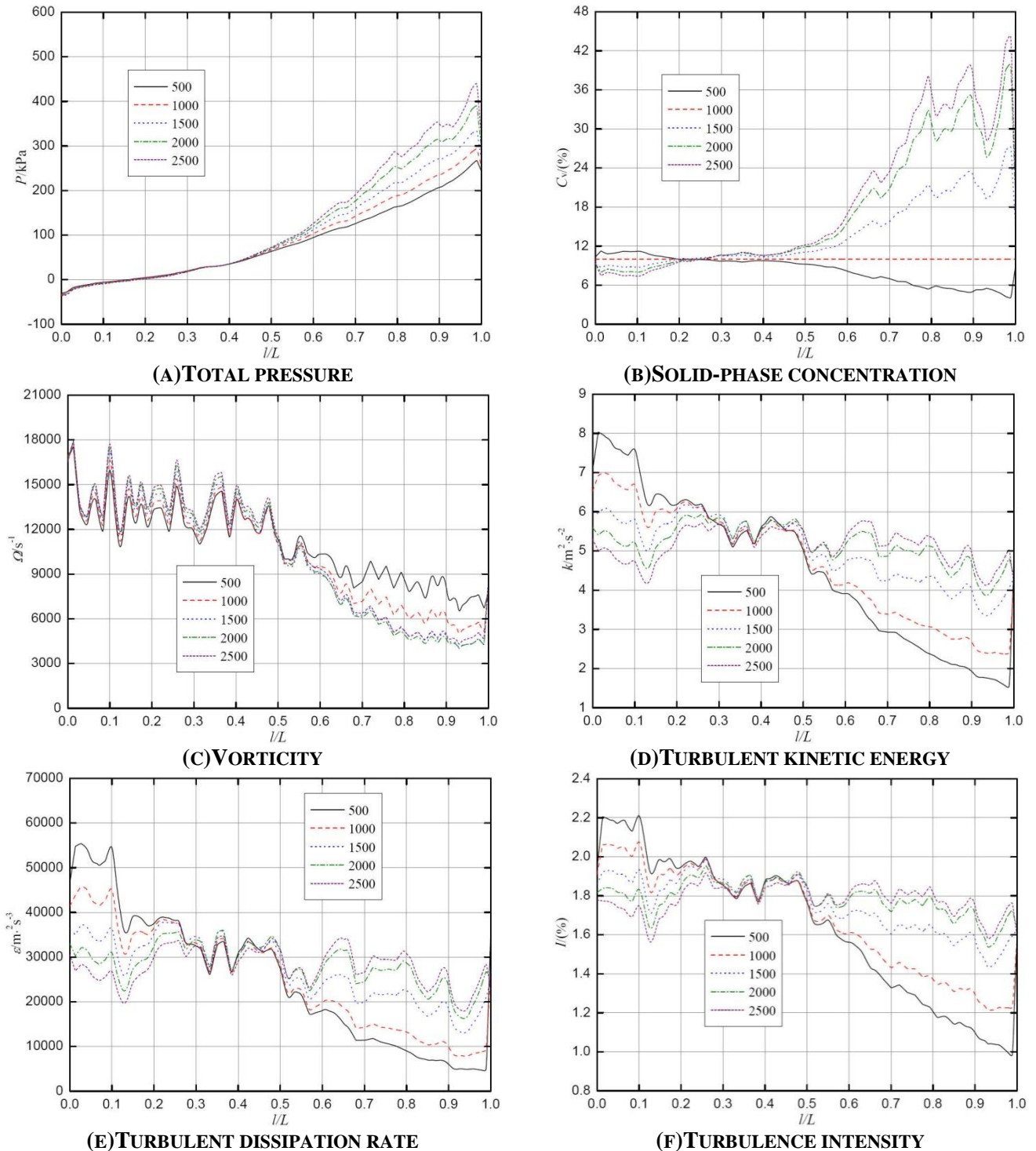


FIG.5 EFFECTS OF PARTICLE DENSITIES ON THE PERFORMANCE PARAMETERS OF BLADE SUCTION SURFACE(kg/m³)

3.4 Particle concentration on the blade pressure surface

Fig. 6 shows the distribution of particle concentration on the blade pressure surface in five densities of delivering solid-phase particles. The figure illustrates that when particle density (500 kg/m^3) is smaller than liquid-phase (water) density, the solid-phase concentrations on two sides of the blade pressure surface are considerably higher; when the density of solid-phase particles (1000 kg/m^3) was equal to liquid-phase density, the distribution of solid-phase concentration on the blade pressure surface was more uniform. This result is clearly related to their similar densities. In three cases where the densities of delivering solid-phase particles were 1500, 2000, and 2500 kg/m^3 , with the increase of the density of delivering solid particles, the distribution area of solid-phase concentration on the pressure surface shrank to the inlet. This finding indicated that the wear area and the wear degree on the blade pressure surface decreased.

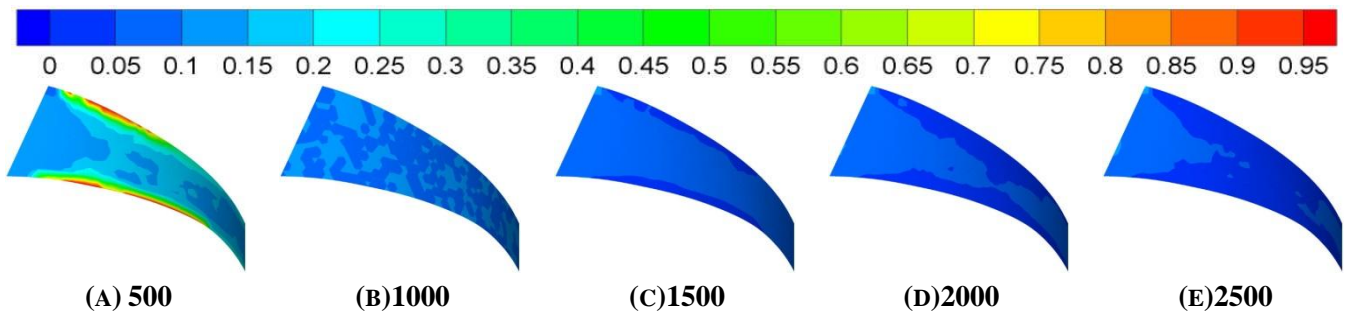


FIG.6 DISTRIBUTION OF THE PARTICLE CONCENTRATIONS ON THE BLADE PRESSURE SURFACE UNDER DIFFERENT PARTICLE DENSITIES (kg/m^3)

3.5 Particle concentration on the blade suction surface

Fig. 7 shows the distribution of particle concentration on the blade suction surface in five densities of delivering solid-phase particles. When particle density (500 kg/m^3) was smaller than the liquid-phase (water) density, the solid-phase concentration on the first half of the blade suction surface was higher than that on the second half of the blade suction surface. The wear was more serious. When the density of solid-phase particles (1000 kg/m^3) was equal to liquid-phase density, the distribution of solid-phase concentration on the blade suction surface was more uniform. Therefore, the degree of wear was also consistent. In three cases where the densities of delivering solid-phase densities were 1500, 2000, and 2500 kg/m^3 , the density of particles was apparently greater than the liquid-phase density. With the increase of the density of delivering solid particles, solid-phase volume fraction on the second half of the suction surface was higher. This finding indicated that the degree of wear on the blade suction surface was constantly increasing.

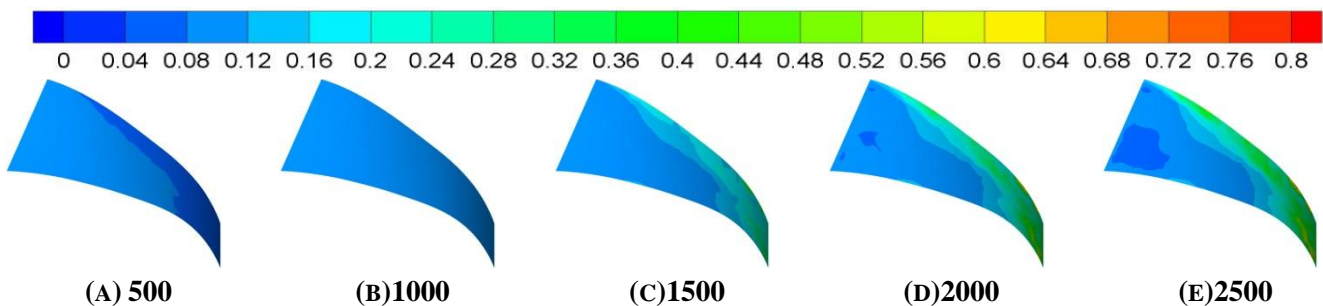


FIG.7 DISTRIBUTION OF PARTICLE CONCENTRATIONS ON THE BLADE SUCTION SURFACE UNDER DIFFERENT PARTICLE DENSITIES (kg/m^3)

3.6 Particle concentration on volute surface

Fig. 8 shows the distribution of particle concentration on volute surface under five different densities of delivering solid-phase particles. When the density of delivering solid particles (1000 kg/m^3) was equal to the liquid-phase density (1000 kg/m^3), solid-phase volume fraction on volute surface was very uniform. The degree of wear in this case was the same. However, when the particle density was smaller or greater than the liquid-phase density ($500, 1500, 2000,$ and 2500 kg/m^3), the solid-phase volume concentration on volute surface was more or less non-uniform. The degrees of wear on volute surface under these four cases were not the same.

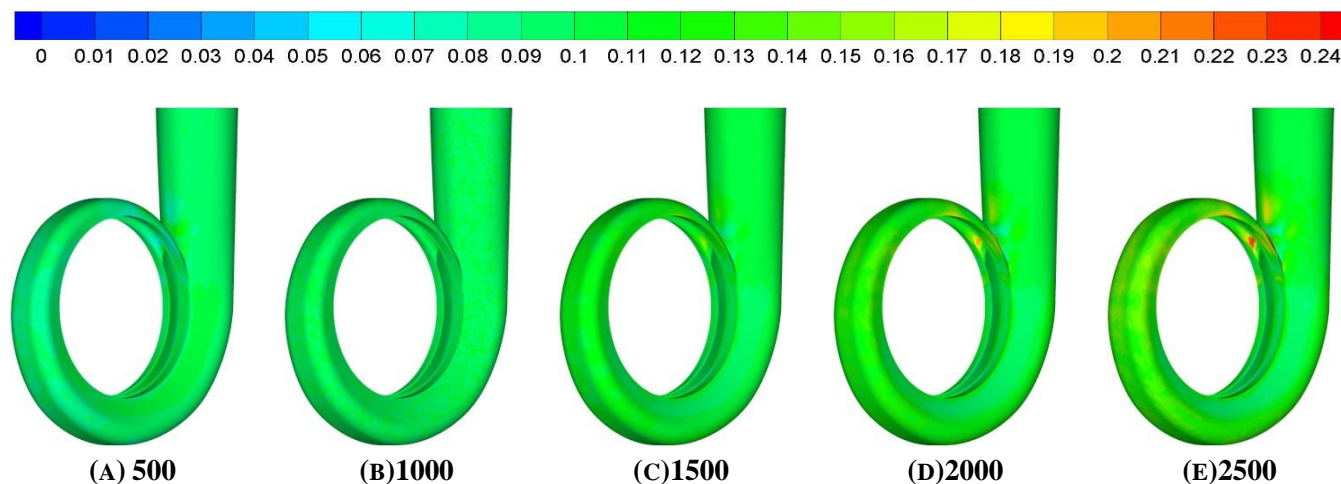


FIG.8 DISTRIBUTION OF PARTICLE CONCENTRATIONS ON VOLUTE SURFACE UNDER DIFFERENT PARTICLE DENSITIES (kg/m^3)

IV. CONCLUSION

- 1) With the increase of the density of solid particles, the total pressure of both the pump inlet and the pump outlet showed a trend of monotonic decline. Pump calculation head curve showed a trend of first declining and then rising, reaching the minimum value of 13.66m when the density of solid particles was 1500kg/m^3 . The pump efficiency curve showed a trend of initial rise and decline and then rise, but its change was not significant. The pump shaft power showed a trend of monotonic rise.
- 2) When particle density was smaller than, equal to, and greater than liquid-phase concentration, solid-phase concentration on the blade pressure surface showed the distribution laws more than, equal to, and smaller than 10%, respectively. With the increase in the density of solid particles, solid-phase concentration on the blade pressure surface showed a gradually declining trend. These findings indicated that the wear and tear was getting smaller and smaller.
- 3) In the middle and late half of the blade suction surface, when the density of solid particles was smaller than that of water, solid-phase concentration on the blade suction surface gradually decreased. This result indicated that the wear and tear was constantly smaller and smaller. In the case where the density of solid particles was greater than water density, solid-phase concentration on the blade suction surface increased gradually. This finding indicated that the wear and tear constantly increased. However, in a small part from the front edge of the blade suction surface, the change trends of both were opposite. This finding showed that the degree of wear was opposite.

ACKNOWLEDGEMENTS

The work was supported by the Zhejiang Provincial Science and Technology Project (No.2015C31129, No.2016C31127), Academic Foundation of Quzhou University (No.XNZQN201508).

REFERENCES

- [1] Engin T, Gur M. Performance characteristics of centrifugal pump impeller with running tip clearance pumping solid-liquid mixtures[J]. Journal of Fluids Engineering, 2001, 123(3): 532-538.
- [2] Gandhi B K, Singh S N, Seshadn V. Effect of speed on the performance characteristics of a centrifugal slurry pump[J]. Journal of Hydraulic Engineering, 2002, 128(2): 225-233.
- [3] Yuan Shouqi, Zhang Peifang, Zhang Jinfeng. Numerical simulation of 3-D dense solid- liquid two- phase turbulent flow in a non-clogging mud pump[J]. Chinese Journal of Mechanical Engineering, 2004, 17(4):623-627.
- [4] Li Yi, Zhu Zuchao, He Weiqiang, et al. Numerical simulation and experimental research on the influence of solid phase characteristics on centrifugal pump performance[J]. Chinese Journal of Mechanical Engineering, 2012, 25(6): 1184-1189.
- [5] Zhang Yuliang, Li Yi, Cui Baoling, et al. Numerical simulation and analysis of solid-liquid two-phase flow in centrifugal pump[J]. Chinese Journal of Mechanical Engineering, 2013, 26(1): 53-60.
- [6] Zhang Yuliang, Li Yi, Zhu Zuchao, et al. Computational analysis of centrifugal pump delivering solid-liquid two-phase flow during startup period[J]. Chinese Journal of Mechanical Engineering, 2014, 27(1): 178-185.

-
- [7] Harry H T, Graeme R A. Experimental study on erosive wear of some metallic materials using Coriolis wear testing approach[J]. *Wear*, 2005, (258): 458-469.
- [8] Veselin B. Erosive wear model of slurry pump impeller[J]. *Journal of Tribology*, 2010, 132(2): 021602.1~5.
- [9] Pagalthivarthi K V, Gupta P K, Tyagi V, et al. CFD prediction of erosion wear in centrifugal slurry pumps for dilute slurry flows[J]. *Journal of Computational Multiphase Flows*, 2011, 3(4): 225-245.
- [10] Dong Xing, Zhang Hailu, Wang Xinyong. Finite element analysis of wear for centrifugal slurry pump[C]. *The 6th International Conference on Mining Science & Technology*, 2009, (1): 1532-1538.
- [11] Li Yi, Zhu Zuchao, He Zhaohui, et al. Abrasion characteristic analyses of solid-liquid two-phase centrifugal pump[J]. *Journal of Thermal Science*, 2010, 20(3): 283-287.
- [12] Sanyal J, Vasquez S, Roy S, et al. Numerical simulation of gas-liquid dynamics in cylindrical bubble column reactors [J]. *Chemical Engineering Science*, 1999, 54(21):5071-5083.